JCI The Journal of Clinical Investigation

Single cell sequencing reveals Hippo signaling as a driver of fibrosis in hidradenitis suppurativa

Kelsey R. van Straalen, … , Lam C. Tsoi, Johann E. Gudjonsson

J Clin Invest. 2023. https://doi.org/10.1172/JCI169225.

Research In-Press Preview Dermatology Inflammation

Graphical abstract

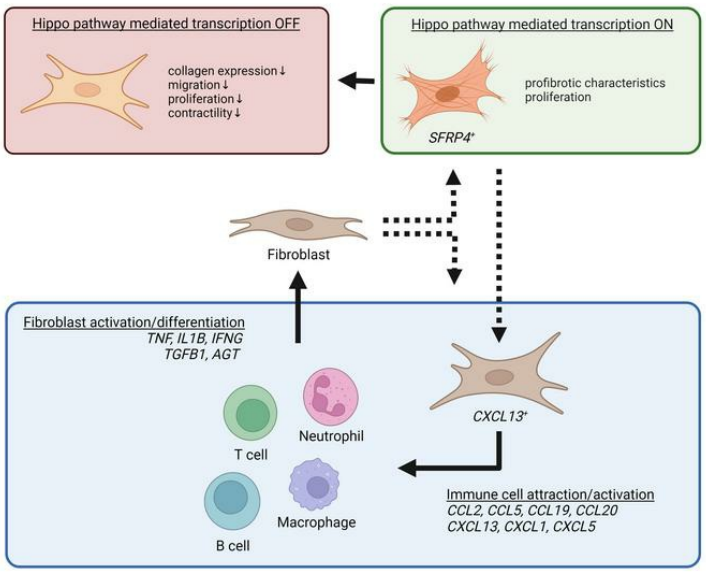

Single cell sequencing reveals Hippo signaling as a driver of fibrosis in hidradenitis suppurativa

Kelsey. R. van Straalen[1], Feiyang Ma[2], Pei-Suen Tsou[2], Olesya Plazyo[1], Mehrnaz Gharaee-Kermani[1,2], Marta Calbet[3], Xianying Xing[1], Mrinal K. Sarkar[1], Ranjitha Uppala[1], Paul W. Harms[1,4], Rachael Wasikowski[1], Lina Nahlawi[1], Mio Nakamura[1], Milad Eshaq[1], Cong Wang[5], Craig Dobry[1], Jeffrey H. Kozlow[6], Jill Cherry-Bukowiec[7], William D. Brodie[2], Kerstin Wolk[8], Özge Uluçkan[3], Megan N. Mattichak[2], Matteo Pellegrini[9], Robert L. Modlin[10], Emanual Maverakis[11], Robert Sabat[8], J. Michelle Kahlenberg[1,2], Allison C. Billi[1], Lam C. Tsoi[1], Johann E. Gudjonsson[1]*

Affiliations:

[1] Department of Dermatology, University of Michigan Medical School, Ann Arbor, Michigan, USA.
[2] Division of Rheumatology, Department of Internal Medicine, University of Michigan Medical School, Ann Arbor, Michigan, USA.
[3] Almirall SA, R&D Center, Sant Feliu de Llobregat, Barcelona, Spain.
[4] Department of Pathology, University of Michigan Medical School, Ann Arbor, Michigan, USA.
[5] Laboratory for Experimental Immunodermatology, Department of Dermatology, Erasmus University Medical Center, Rotterdam, the Netherlands.
[6] Division of Plastic Surgery, Dept. of Surgery, University of Michigan Medical School, Ann Arbor, Michigan, USA.
[7] Section of General Surgery, Dept. of Surgery, University of Michigan Medical School, Ann Arbor, Michigan, USA.
[8] Interdisciplinary group Molecular Immunopathology, Dermatology/Medical Immunology, Charité – Universitätsmedizin Berlin; Berlin, Germany
[9] Department of Molecular, Cell, & Developmental Biology. University of California Los Angeles (UCLA), California, USA.
[10] Department of Dermatology, University of California Los Angeles (UCLA), California, USA.
[11] Department of Dermatology, University of California, Sacramento, California, USA.

***Corresponding author:**
Johann E. Gudjonsson
Department of Dermatology
University of Michigan
1910 Taubman Center
1500 E. Medical Center Drive
Ann Arbor, Michigan, 48109, USA.
Phone: 734 615 4508
Email: johanng@med.umich.edu

Conflict of interest statement

KRvS, FM, PST, OP, MGK, XX, MKS, RU, PWH, RW, LN, ME, CW, CD, JHK, JCB, WDB, ÖU, MNM, MP, RLM, EM, ACB, LCT, and JEG report no competing interests for this work. MC is an employee of Almirall, S.A. MN conducts research for Anaptysbio, Argenx, Bristol-Myer-Squibb, Galderma, Pfizer, and Regeneron. KW has received research grants, consulting honoraria or lecturer's honoraria from AbbVie, Novartis Pharma, Sanofi-Aventis, and MoonLake Immunotherapeutics. RS has received research grants, scientific awards, or honoraria

for participation in advisory boards, clinical trials or as speaker for one or more of the following: AbbVie, Bayer, Boehringer Ingelheim Pharma, CSL Behring, ICON, Incyte, Janssen-Cilag, La Roche-Posay Laboratoire Dermatologique, MoonLake Immunotherapeutics, Novartis Pharma, Parexel, Sanofi-Aventis, and UCB Pharma. JMK has received grants from Janssen, Bristol Myers Squibb, Q32 bio, ROME therapeutics, Ventus Therapeutics and participated in consulting/advisory boards for BMS, AstraZeneca, EMD Serano, Ventus Therapeutics, Eli Lilly, GlaxoSmithKline, Lupus Therapeutics, and Gilead.

ABSTRACT

Hidradenitis suppurativa (HS) is a chronic inflammatory disease characterized by abscesses, nodules, dissecting/draining tunnels, and extensive fibrosis. Here, we integrate single-cell RNA sequencing, spatial transcriptomics, and immunostaining to provide an unprecedented view of the pathogenesis of chronic HS, characterizing the main cellular players, and defining their interactions. We found a striking layering of the chronic HS infiltrate and identified the contribution of two fibroblast subtypes (*SFRP4*$^{+}$ and *CXCL13*$^{+}$) in orchestrating this compartmentalized immune response. We further demonstrated the central role of the Hippo pathway in promoting extensive fibrosis in HS and provided pre-clinical evidence that the pro-fibrotic fibroblast response in HS can be modulated through inhibition of this pathway. These data provide insights into key aspects of HS pathogenesis with broad therapeutic implications.

INTRODUCTION

Hidradenitis suppurativa (HS) is a chronic inflammatory disease of the skin that affects 1% of the general population (1). The disease is characterized by acute, recurrent inflammatory nodules and painful abscesses originating from the hair follicles, typically arising in the axillae and groin (2, 3). Later stages of HS are marked by chronic, persistent inflammation accompanied by dermal tunnel (sinus tract) formation and extensive fibrosis (2, 3).

While the exact pathogenesis of HS remains unknown, genetic predisposition and environmental factors such as cigarette smoking and obesity may contribute to the disease (2, 4–6). The primary pathogenic event is thought to be infundibular hyperplasia arising from an intrinsic keratinocyte defect (2, 7). Subsequent cyst formation and rupture induce acute inflammation, characterized by a mixed immune infiltrate of neutrophils, macrophages, dendritic cells, and T and B cells and increased expression of a battery of pro-inflammatory cytokines including IL-1β, IL-17, and TNF-α (2, 8). Chronic lesions are thought to develop upon repeated rupture or failure to clear the inflammatory follicle contents. These lesions show a shift in immune cell composition marked by a more prominent B cell and plasma cell components (9). Dermal tunnels are a hallmark of these chronic lesions, yet the processes leading to their development remain unknown. Fibrosis is a prominent clinical feature of long-standing hidradenitis suppurativa (2). The relationship of fibrosis to the HS inflammatory response and the mechanisms involved have not been characterized but are of high importance, as fibrosis may interfere with drug penetration and impact overall treatment response (2).

Treatment options for this debilitating disease remain limited, with the only FDA-approved therapy (adalimumab) achieving clinical response in only 40-60% of patients (10). Response rates among newer, repurposed, biological therapies in large clinical trials have so far

failed to exceed this (10, 11). A major barrier to the identification of treatment targets and successful clinical translation is our lack of understanding of the interplay between the different cell types – both immune and stromal – in the HS microenvironment. The contribution of stromal cells, while clearly implicated by clinical symptoms of tissue destruction and fibrosis, has only been explored to a limited extent (12, 13).

In this paper, we use single-cell RNA sequencing (scRNAseq) and spatial transcriptomics to define the cellular composition and spatial architecture of the infiltrate in chronic HS lesions. Our results provide an unprecedented view of HS pathology, demonstrating how stromal-immune cell interactions contribute to the inflammatory network at the site of disease and identifying a pathway implicated in HS fibrosis that may serve as a potential target for future therapeutic interventions.

RESULTS

Chronic HS lesions show altered cell composition and complex layered architecture

To understand the cell composition of healthy and chronic HS lesional skin, we performed single-cell RNA sequencing (scRNAseq) on cells isolated from chronic lesional skin of five HS patients and eight healthy donors (normal skin, NS). We collected 31,716 cells and identified 21 clusters that we annotated as 11 distinct primary cell types: keratinocytes (KCs), melanocytes, eccrine gland cells, endothelial cells, fibroblasts (FBs), smooth muscle cells, T cells, myeloid cells, mast cells, B cells, and plasma cells (Figure 1A, Supplemental Figure 1A). Interestingly, for all major stromal cell types, including keratinocytes and fibroblasts, the UMAP showed distinct separation between HS and NS cells, suggesting fundamental transcriptomic changes in

the HS-associated cell types (Figure 1A-B). Analysis of the disease composition for each cell type revealed an increased proportion of KCs and immune cells, particularly T cells, B cells, plasma cells, and myeloid cells in HS (Figure 1C). This high number of KCs and massive immune cell infiltration, obtained from biopsies in chronic inflammatory lesions, resulted in a relative decreased proportion of eccrine gland cells, FBs, and smooth muscle cells. Figure 1D shows the expression of relevant marker genes for each cell type. These results indicate that chronic HS is characterized by both the accumulation of an abnormal immune infiltrate and a marked transcriptomic shift in all major stromal cell types.

We performed spatial transcriptomics on 4 samples to elucidate the spatial organization of the identified cell types within chronic HS lesional skin. Subsequently, we deconvoluted the RNA expression in each spot with the scRNAseq gene expression of the major cell types to identify the cell type composition in each capture spot (Supplemental Figure 1B). As expected, KCs were primarily detected in the epidermis. Interestingly, a layered architecture was seen in chronic HS lesions. Myeloid cells were localized primarily within a large focus of dense inflammation, where T cells are dispersed throughout the infiltrate (Fig 1E-F and Supplemental Figure 1C). B cells were found in clusters at the edge of the infiltrate. (Figure 1E-F). The inflammatory infiltrate was demarcated by a layer of FBs, with plasma cells found primarily outside of the fibroblast zone (Figure 1F). Figure 1G demonstrates the localization of *COL1A1*, *PTPRC* (CD45), *KRT1*, and *CDH5* (vascular endothelial cadherin). Immunohistochemistry (IHC) corroborated this layered arrangement of infiltrating immune cells and stromal cells centering around a ruptured tunnel or abscess (Figure 1H).

To analyze the differences in cell-cell communication between HS and healthy skin, we performed ligand-receptor analysis using CellPhoneDB and analyzed the ligand-receptor pairs

with higher interaction scores in HS than NS. This identified myeloid cells, KCs, FBs, endothelial cells, smooth muscle cells, and to lesser extent T cells, as the major putative cell interactors in lesional HS skin (Figure 2A). Growth factor and cytokine interactions between myeloid cells, KCs, FBs, endothelial cells, and smooth muscle cells are plotted in Figure 2B-E (Supplemental Figure 2 for the smooth muscle cells). Myeloid cells showed expression of several growth factors (*VEGFA, VEGFB, PDGFB,* and *PDGFA*), which link to their respective receptors on KCs, FBs, endothelial cells, and smooth muscle cells, potentially stimulating the proliferation of these cells (Figure 2B). KCs expressed several chemokines (*CXCL9, CXCL10, CXCL11*) and cytokines (*IL1, IL15*) capable of interacting with their respective receptors on myeloid cells and fibroblasts (Figure 2C). FBs expressed a plethora of chemokines (e.g., *CCL19*, *CCL20*, *CXCL2*, *CXCL12*) that bind to receptors on myeloid cells, suggesting an important role for FBs in recruiting immune cells to the HS infiltrate (Figure 2D). Both endothelial cells and smooth muscle cells produced diverse chemokines and growth factors interacting with their respective receptors on KCs, FBs, and myeloid cells (Figure 2E and Supplemental Figure 2). Moreover, multiple chemokines produced by these cell types were predicted to be scavenged from the micro-environment by KCs and FBs through interaction with atypical chemokine receptors *ACKR2, ACKR3,* and *ACKR4* (14, 15).

cDC2B cells and macrophages can promote neutrophil activation and degranulation in HS skin.

To examine the heterogeneity in myeloid cells, we subclustered the myeloid cells and annotated six subpopulations: Langerhans cells (LC), classical type 1 dendritic cells (cDC1), classical type 2 dendritic cell subset A (cDC2A), classical type 2 dendritic cell subset B (cDC2B),

plasmacytoid dendritic cells (pDC), and macrophages (Mac) (Figure 3A). Analysis of the disease composition revealed that pDCs and cDC2B cells were mainly derived from HS lesional skin, which also showed a relative decrease in LCs compared with healthy skin (Figure 3B-C). Characteristic marker genes for all subpopulations are shown in Figure 3D. IHC revealed distinct spatial localization for many of the myeloid cell subtypes within the layered architecture of chronic HS lesional skin. As expected, LCs were found primarily within the epidermis (Figure 3E). Classical type 1 dendritic cells were found predominantly at the centre and edges of the infiltrate, whereas cDC2A were found in small clusters within the infiltrate, and the cDC2B, pDCs, and macrophages were dispersed throughout the infiltrate (Figure 3E). While our single cell skin digestion protocol precludes capture of neutrophils, analysis of the enriched biological processes of the cDC2B and macrophage subtypes revealed their extensive involvement in neutrophil activation and degranulation (Figure 3F-G). pDCs were found to be highly transcriptionally active and show upregulation of general protein translation pathways (Figure 3H).

IL17$^+$ T cells contribute to the production of both *IL17A* and *IL17F* in HS lesional skin

To assess for dysregulation of T cell subsets in HS, we aimed to characterize the T cell subtypes found in our data. We identified six T/NK cell subtypes in HS lesional and healthy skin: CD4$^+$ central memory T cells (CD4Tcm), regulatory T cells (Treg), T follicular helper cells (Tfh), IL17$^+$ T cells (T17), CD8$^+$ effector memory T cells (CD8Tem), and natural killer cells (NK) (Figure 3I). Analysis of the disease composition revealed an increased proportion of Tfh, T17, and NK cells in HS (Figure 3J-K). Similar to previously published data we found no difference in the proportion of CD8Tem cells in HS lesional skin compared with healthy skin (16, 17).

Marker genes for the identified T cell subtypes are shown in Figure 3L. To identify the nature of the $IL17^+$ T cells we generated correlation plots between *IL17A*, *CD4*, and *CD8A*, revealing that $CD4^+$ T cells and $CD8^+$ T cells are likely both a source of *IL17A* in HS lesional skin (Figure 3M-N). Moreover, these cells were found to express both *IL17A* and *IL17F (*Figure 3O*).*

As B cells are a prominent component of chronic HS lesions and the formation of tertiary lymphoid structures has been described, the presence of Tfh cells in our HS samples was intriguing (8, 9). T follicular helper cells are known for their interaction with B cells within lymphoid organs rather than in inflamed peripheral tissue, where this role is normally executed by T peripheral helper cells (Tph) (18). Thus, we assessed the expression of several shared and unique markers of Tfh and Tph lineages to uncover clues to the role of these two cell subtypes in HS lesions (Supplemental Figure 3). The clear absence of *CCR2* and *CCR5* expression in this cell cluster supported the annotation of these cells as Tfh rather than Tph cells (Supplemental Figure 3). The expression of *CXCR5* and Tfh-defining transcription factor *BCL6* in at least a subset of these cells suggests the presence of mature Tfh cells in HS lesional skin (Supplemental Figure 3). These data substantiate a role for this *CXCL13* expressing T cell population in the previously identified formation of tertiary lymphoid structures in chronic HS lesional skin (Supplemental Figure 3) (8).

Distinct epidermal KC maturation states in HS reflect different cytokine responses

The clear separation of HS and NS epidermal KCs in Figure 1A-B indicates transcriptomic changes in HS KCs suggestive of altered cell function. To further characterize these differences, we subclustered the KC population and annotated basal, spinous, and supraspinous KCs based on marker gene expression (Figure 4A- 4C). Next, we performed differential gene expression

analysis between HS and NS KCs within each maturation subtype to identify the top distinguishing transcripts (Figure 4D). Across all epidermal layers, HS KCs showed markedly increased expression of antimicrobial/antifungal S100 genes (*S100A7, S100A8,* and *S100A9*) and proliferation genes (*KRT6A* and *KRT16*). HS spinous and supraspinous KCs showed a loss of expression of desmosomal cadherins *DSG1* and *DSC1*, as well as *KRT2* (Figure 4D).

We next sought to identify the inflammatory drivers of these subtypes by interrogating cells of each maturation subtype for genes known to be induced in cultured KCs by certain cytokines such as TNF, IL-17A, IL-36γ, and type I IFN (IFNα). HS KCs showed heightened scores for TNF, IL-17A, IL-36γ, IFNγ, and type I IFN responses in all three maturation subtypes compared with NS skin (Figure 4E). HS KCs showed a striking increase in TNF, IL-1β, and IL-17A response scores from spinous and supraspinous KCs, whereas NS KCs showed a minimal increase. A prominent increase from spinous to supraspinous KCs was also observed for IL-36γ and IFNγ responses in both HS and NS KCs, albeit on average higher for HS KCs.

To address the distinct separation of the NS and HS KCs, particularly the spinous and supraspinous KCs, we performed pseudotime analyses using Monocle to examine the NS and HS KC maturation pathways separately. This arranged both HS KCs (Figure 4F-G) and NS KCs (Supplemental Figure 4A-B) into linear trajectories in the expected direction of basal-spinous-supraspinous maturation. Next, to identify potential cytokines that drive maturation of HS and NS KCs, variable genes along either the NS or HS pseudotime were divided into five expression patterns (clusters, HS KCs in Supplemental Figure 4C and NS KCs in Supplemental Figure 4D). We then inferred the upstream regulators for the genes in each cluster using Ingenuity Pathway Analysis (IPA). For each upstream regulator, we calculated a module score using all target genes across the five expression patterns/clusters and the correlation between the module scores for

each upstream regulator and the pseudotime defined by the Monocle analysis (Figure 4H). These analyses showed that module scores for IL-17A, IL-22, IL-1α, IL-1β, and IL-6 were positively correlated with HS KC pseudotime, whereas IL-4 and PF4 correlated with NS KC pseudotime (Figure 4I). Subsequently, to validate the cytokines driving HS keratinocyte maturation, we calculated module scores using genes induced in cultured KCs stimulated by individual cytokines; IL-17A, IL-22, IL-1α, IL-1β and IL-6. The module scores for these five cytokines were highly correlated with the HS but not NS KC pseudotime, consistent with the results obtained in the IPA analysis (Figure 4I and Supplemental Figure 4E).

Taken together these results suggest that the altered KC maturation seen in chronic HS lesions is driven by local cytokines, particularly IL-17A, IL-22, IL-1α, -1β, and IL-6. Their activation and subsequent functional responses are mainly driven by TNF, IL-17A, IL-36γ, IFNγ, and type I IFNs.

Proliferative blood vessels can promote immune cell infiltration in HS chronic lesional skin

Chronic HS is characterized both by a massive influx of immune cells as well as clinically prominent angiogenesis. As expected, IHC and IF staining for CD31 (endothelial cells) and ACTA2 (vascular mural cells) showed prominent vascularization of HS chronic skin lesions (Supplemental Figure 5A-B). Subclustering the endothelial cells identified five vascular endothelial clusters (EC0, 1, 2, 4, and 5) and one lymphatic endothelial cluster (EC3) (Supplemental Figure 5C). Both EC4 and EC5 were nearly completely derived from HS lesional skin (Supplemental Figure 5D-E). These HS-associated subclusters showed an immunologically active phenotype, with the expression of immune-activated genes e.g., *ICAM1*, *SELE*, *IL6*, and *CCL14*. The HS-associated subclusters showed expression of *HLA-DRB5* and *HLA-DRA*, which

could allow them to orient the HS T cell response towards a Th17 pro-inflammatory response (19) (Supplemental Figure 5F-G). Moreover, EC5 subcluster markers *COL4A1*, *COL4A2*, and *SPARC* are associated with vascular remodeling and angiogenesis (Supplemental Figure 5F). Interrogating the enriched biological processes of the EC4 and EC5 subclusters demonstrated the EC4 to be particularly immunologically active (Supplemental Figure 5H). The EC5 subcluster is highly transcriptionally active showing upregulation of several protein translation processes (Supplemental Figure 5I).

As smooth muscle cells integrate with endothelial cells to form the vasculature, we next examined this cell subset. We identified six smooth muscle subclusters with two subclusters, SMC0 and SMC6, almost exclusively derived from HS lesional skin (Supplemental Figure 6A-C). These two subclusters both showed expression of *IGFBP4*, *IGFBP2*, *COL4A1*, and *TIMP1*, genes associated with vascular smooth muscle cell proliferation and migration (Supplemental Figure 6D). In addition, SMC6 showed a proinflammatory phenotype with increased expression of *CCL2*, CXCL2, and *CXCL3* (Supplemental Figure 6D). Analysis of the enriched biological processes showed both SMC subclusters to be highly transcriptionally active, with SMC6 demonstrating prominent activation via local cytokine stimuli (Supplemental Figure 6E-F).

In summary, these results support the clinical signs of active vascular proliferation seen in chronic HS lesions and demonstrate the role of immunologically active endothelial cells in the massive infiltration of immune cells in chronic HS lesions.

Functionally diverse FB subtypes likely drive HS inflammation and fibrosis

While extensive fibrosis is a hallmark of chronic HS, as demonstrated by trichrome staining (Figure 5A), FBs have not been studied in detail (2, 12, 13). Therefore, we aimed to further

characterize the differences between HS and NS FBs. We identified 11 clusters which we annotated into six FB subtypes according to previously published marker genes: *SFRP2*$^+$, *LSP1*$^+$, *COL11A*$^+$, *RAMP1*$^+$, *SFRP4*$^+$, and *CXCL13*$^+$ FBs (Figure 5B) (20). Two of these subtypes, *SFRP4*$^+$ and *CXCL13*$^+$ FBs, were derived nearly exclusively from HS samples (Figure 5C). The top three marker genes for all FB subtypes are shown in Figure 5D. The *SFRP4*$^+$ and *CXCL13*$^+$ FBs were not only specifically derived from HS samples but were also found in a profoundly increased proportion compared to the other FB subtypes in these samples (Figure 5E). Quantitative PCR corroborated increased expression of specific marker genes of these populations in primary FBs derived from lesional HS versus NS skin (Supplemental Figure 7A). Co-staining of CXCL13 and either vimentin (FB marker) or CD3 (T cell) by immunofluorescence demonstrated more prominent protein expression of CXCL13 among FBs than T cells in HS lesional skin (Figure 5F). IHC further confirmed the presence of the identified FB subtypes in HS lesional skin (Figure 5G). Both the *CXCL13*$^+$ and the *SFRP4*$^+$ FBs were found to demarcate the edges of the inflammatory infiltrate (Figure 5G and Figure 1F). Dot, violin and feature plots of expression levels of the most prominently expressed collagen genes revealed the strongest expression among the *SFRP4*$^+$ FBs (Figure 5H, Supplemental Figure 8 A-B). Taken together with a high ECM module score (Figure 5I) and high expression of *ACTA2* (actin alpha 2, smooth muscle,Figure 5J), *SFRP4*$^+$ FBs were identified as myofibroblasts.

To further characterize the functions of these HS-associated *CXCL13*$^+$ and *SFRP4*$^+$ FBs, we performed analysis of upregulated canonical pathways and enriched gene ontology biological processes. As expected, the *SFRP4*$^+$ subtype showed functions associated with fibrosis and extracellular matrix formation (Supplemental Figure 8C-D). Additionally, this subtype demonstrated immunological functions enriched for neutrophil activation. Canonical pathway

analysis of the *CXCL13*$^+$ FBs identified numerous upregulated signaling pathways, most prominently Oncostatin M (OSM) and IL-17A/F associated pathways (Supplemental Figure 8E). Upregulated biological processes showed these cells to be highly transcriptionally active, with immunological functions aimed at attracting and activating neutrophils and lymphocytes (Supplemental Figure 8F). Ligand-receptor analysis for chemokines and cytokines expressed by the *SFRP4*$^+$ and *CXCL13*$^+$ FBs revealed that both subtypes are engaged in extensive communication networks with different immune cells within the HS infiltrate (SupplementalFigure 5K), although the expression of these cytokines and chemokines is highest in the *CXCL13*$^+$ FBs (Supplemental Figure 6L). Furthermore, the *SFRP4*$^+$ and *CXCL13*$^+$ FBs contribute to a complex interplay among different MMPs, collagens, and laminins derived from the distinct HS-associated cell subtypes to promote extracellular matrix deposition and remodeling (Supplemental Figure 8M-N). Taken together, these data support a prominent proinflammatory and remodeling role for the *CXCL13*$^+$ FBs and implicate *SFRP4*$^+$ FBs as myofibroblasts, with a prominent expression of *COL1A1* and *ACTA2*, driving fibrosis in chronic HS.

Recent clinical and pre-clinical studies have implicated the contribution of Hippo signaling pathway components in fibrotic diseases in many organs including the lung, heart, and skin (21–23). To investigate the role of Hippo pathway signaling in HS fibrosis we assessed the expression of Hippo pathway signaling factors in our fibroblast subsets. This revealed increased expression of both Hippo pathway transcriptional coactivators and transcription factors (*YAP1*, *WWTR1*, and *TEAD1-4* (Figure 6A) as well as known target genes (*CTGF*, *CYR61*, and *COL8A1*) (Figure 6B) primarily among the *SFRP4*$^+$ population. Protein expression of YAP,

WWTR1/TAZ, TEAD1, TEAD2, and TEAD4 was confirmed in HS lesional skin FBs by IHC (Figure 6C).

To further support the hypothesis that Hippo pathway signaling is involved in the activation of HS myofibroblasts we performed upstream regulator analysis. Indeed, in addition to well-known pro-fibrotic markers such as TGF-β and angiotensinogen (AGT, which has previously been identified as a critical component in cardiac and pulmonary fibrosis (20, 24)), we identified several factors belonging to the Hippo pathway (*YAP1*, *WWTR1*, and *TEAD2*), particularly among the *SFRP4*$^+$ myofibroblasts (Figure 6D and Supplemental Figure 9A). In addition, the key HS-associated cytokines TNF, IL-1β, IFNγ, and IL-6 were found to be highly activated upstream regulators for both the *CXCL13*$^+$ and *SFRP4*$^+$ subtypes (Supplemental Figure 9B).

Next, we performed pseudotime analysis to identify if Hippo pathway transcription factors were associated with the activation and development of the *SFRP4*$^+$ and *CXCL13*$^+$ FB phenotypes, using the underlying identified clusters (Figure 6E). These clusters were arranged into a linear trajectory in the direction from the *SFRP2*$^+$ to *SFRP4*$^+$, with a less clearly defined *CXCL13*$^+$ endpoint (Figure 6F-G). Not only *TGFB*, *TNF*, *IFNG*, and *IL1B* (Figure 6H) but also the Hippo pathway transcriptional regulator *YAP*, its coactivator *WWTR1*, and transcription factors *TEAD1-4* were found to be highly correlated with the FB pseudotime (Figure 6I). Interrogating ataq seq data demonstrated increased chromatin accessibility in the *WWTR1*, *TEAD1* and *COL8A1* regions of lesional HS fibroblasts compared with and non-lesional and healthy skin fibroblasts (Supplemental Figure 10) further supporting the activation of the Hippo pathway in HS lesional fibroblasts.

To uncover the functional role of Hippo signaling (Figure 7A) in HS fibrosis, we performed *ex vivo* experiments using primary dermal FBs obtained from chronic HS lesions. FBs were stimulated with either TRULI (which blocks YAP phosphorylation, thereby activating YAP-mediated transcriptional coactivation (25)) and verteporfin (which disrupts YAP-TEAD interaction, resulting in YAP target inhibition (26)). Verteporfin significantly reduced both protein and RNA expression of collagen I and, to a lesser extent, smooth muscle actin (SMA/*ACTA2)* in HS FBs (Figure 7B-C). Verteporfin stimulation also significantly inhibited HS FB contractility in the gel contraction assays (Figure 7D) and resulted in a significant dose-dependent reduction of both proliferation and migration of HS FBs (Figure 7E-F). In contrast, stimulation of YAP transcriptional activity with TRULI resulted in a non-significant increased RNA expression of smooth muscle actin (*ACTA2*) and collagen I (*COL1A1*) (Figure 7B). TRULI treatment did significantly induce *CTGF* expression (Figure 7B). Treatment with TRULI also significantly increased proliferation but failed to further increase either migration or gel contraction (Figure 7D-F). Performing the same experiments with healthy control fibroblasts showed similar results upon TRULI or verteporfin stimulation as HS fibroblasts but to a lesser extent (Supplemental Figure 11). In particular, upregulation of this pathway by TRULI seemed to result in a more limited upregulation of collagen 1 or smooth muscle actin RNA and protein compared with HS FBs (Figure 7B and Supplemental Figure 11A-B). Moreover, TRULI was unable to induce further proliferation of healthy fibroblasts, which was already significantly lower than that of HS FBs.

To assess the relevance of the Hippo pathway to pro-inflammatory characteristics of HS FBs, we examined the expression of several cytokines and chemokines after TRULI and verteporfin stimulation alone or in combination with single cytokine stimulations. Overall,

neither TRULI nor verteporfin significantly affected the expression of *CCL2*, *CCL5*, *CXCL1*, *CXCL8,* or *IL6* in HS FBs in response to stimulation with the previously identified upstream regulators IL-1β, TNF, or IFNγ (Figure 7G). These experiments indicate that the Hippo pathway is involved in HS myofibroblast differentiation but dispensable for the HS-specific *CXCL13*$^{+}$ FB phenotype.

Taken together, these data support a role for the Hippo pathway in promoting the extensive fibrosis of HS and demonstrate that inhibition of this pathway can modulate the pro-fibrotic characteristics of HS FBs, independent of their pro-inflammatory characteristics.

Ligand-receptor analysis reveals cell subtype specific networks in HS lesional skin.

Given the marked shifts in cell subtype composition in chronic HS lesional skin, we analyzed the cell-cell communication between cell subtypes in HS skin. Intriguingly, the greatest number of ligand-receptor pairs were found for *SFRP4*$^{+}$ FB subtype, particularly in connection with the EC4 and EC5 endothelial cell subsets (Figure 8A-B). Plotting the expression of their ligands and receptors demonstrates how *SFRP4*$^{+}$ FBs express *VEGFD*, *FGF7*, *IGF1* providing strong angiogenic stimuli to both the immunologically active EC4 and transcriptionally active EC5 subtypes (Figure 8C). In line with its pro-inflammatory phenotype, the *CXCL13*$^{+}$ FB subtype was found to express a multitude of angiogenic chemokines *CCL3*, *CCL5*, *CXCL1*, *CXCL5*, *CXCL8* (27, 28). In turn, EC4 and EC5 use distinct signaling molecules to communicate with the FB subtypes. EC5 expresses *SEMA4A* and *PDGFB,* promoting proliferation and pro-fibrotic characteristics in FBs (29, 30). In contrast, the EC4 subcluster expresses *CXCL11* and *IL15*, which have been demonstrated to have antifibrotic properties in several animal models of fibrotic disease (27, 31). Additionally, the EC subclusters also express either *CCL14* or *CXCL12*, which

bind to their respective receptors *CCR1* and *CXCR4* on cDC2B cells, facilitating their trans-endothelial migration and aiding survival (32). These cDC2B cells in turn communicate with both endothelial cell clusters through *CXCL8*, *IL1B*, and *CCL3* to promote angiogenesis and increase vascular permeability (33). Interestingly, cDC2B cells also express *DLL1*, which binds to *NOTCH* receptors present on all endothelial and FB subtypes to promote angiogenesis and collagen release, respectively (34).

In summary, HS lesional skin hosts complex cellular crosstalk in which cDC2B cells stimulate endothelial cells and FBs which in turn attract and activate cDC2B cells, ultimately resulting in a dense immune infiltrate accompanied by extensive fibrosis and angiogenesis.

DISCUSSION

Here, through a combination of single-cell RNA sequencing, spatial transcriptomics, and immunostaining, we provided several critical insights into the pathogenesis of HS. We reveal a highly structured and compartmentalized inflammatory response in chronic HS, and we demonstrate how this compartmentalization is orchestrated through cellular crosstalk between immune cells and stromal cells. We further establish that two stromal subtypes enriched in HS lesional skin, *CXCL13*$^{+}$ and *SFRP4*$^{+}$ FBs, play a major role in shaping and perpetuating the inflammatory response in HS through secretion of chemokines that recruit B cells and myeloid cells, as well as driving the extensive fibrosis that is characteristic of longstanding HS.

Our data characterize the cellular crosstalk likely responsible for immune compartmentalization in HS skin. At the center of HS lesions, including abscesses and sinus tracts, neutrophils are found in close proximity around ruptured tunnel fragments (Figure 1F,H) (2). Here, they likely represent the first line of defense in response to damage-associated

molecular patterns (DAMPs), pathogen-associated molecular patterns (PAMPs), and complement factors (2, 35). Their primary antimicrobial functions of phagocytosis, degranulation, and the release of neutrophil extracellular traps (NETs) result in the characteristic purulent drainage from abscesses and tunnels (36). We found other immune cell populations such as cDC2B, pDCs, macrophages, and T cells near the neutrophil infiltration (Figure 1F, H and Figure 3E). Both cDC1 and cDC2 subtypes contribute to the respective induction of Th1 and Th17 subtypes (37), the latter of which was enriched in HS in our data (Fig 3K), consistent with previous observations. In contrast, B cells were found primarily at the edges of the infiltrate near the demarcating layer primarily consisting of *CXCL13*$^{+}$ and *SFRP4*$^{+}$ FBs (Figure 1F, H and Figure 5G). In addition, *CXCL13*$^{+}$ fibroblasts expressed multiple other chemokines (i.e., *CXCL12*, *CCL19*) which likely further contribute to the spatial localization of the B cell population at the periphery of actively inflamed abscesses and sinus tracts. This cross-talk is likely bi-directional, with our previous study demonstrating the expression of e.g. *TGFB1* by B and plasma cells in chronic lesional skin (9). Moreover, B cells have also been shown to be able to directly induce fibrosis in patients with IgG4-related disease (38). *SFRP4*$^{+}$ myofibroblasts were found at the edge of the lesions, close to B cell populations, contributing to the fibrotic zone surrounding the actively inflamed areas in the skin. Within this zone, clusters of B cells, T cells, and plasma cells were found (Figure 1F, H), suggestive of tertiary lymphoid-like structures.

These tertiary lymphoid-like structures (TLS) have previously been described in chronic HS lesions, and our current data suggests that their formation might be in part driven by *CXCL13*$^{+}$ FBs (8). TLS formation involves recruitment and homing of T cells through CCL19 and CCL21, and chemoattraction and maintenance of B cells through CXCL13-CXCR5

interactions (39, 40). Our data support such a mechanism in HS, with both *CCL19* and *CXCL13* being expressed by the HS-enriched *CXCL13*$^+$ FB subtype (Supplemental Figure 8E-F). Differentiation of TLS-associated fibroblasts is a known phenomenon in response to inflammatory triggers such as TNF, IL-17, and IL-23 (41, 42). These cytokines play a prominent role in the pathogenesis of HS (2), and both TNF and, to a lesser extent, IL-17 were identified as upstream regulators of *CXCL13*$^+$ activation in our data. Remarkably, a large proportion of *CXCL13*$^+$ FBs showed higher expression of *CXCL13* than Tfh cells, likely reflecting the importance of the *CXCL13*$^+$ FB subtype to the migration of B cells, and their spatial localization at the periphery of the actively inflamed areas of chronic HS lesions, potentially as TLSs. In addition, the expression of *CXCL12* and *IL7* by *CXCL13*$^+$ FBs (Supplemental Figure 8E-F) may contribute to chemotaxis and survival of both B and T cells in HS lesions. TLSs actively regulate local immune responses, influence disease progression, and likely contribute to the large number of B and plasma cells present in chronic HS lesions (9, 43), potentially making them a therapeutic target in HS. Furthermore, *CXCL13*$^+$ fibroblasts may further promote inflammatory responses through the expression of a wide range of cytokines and chemokines, including the neutrophil chemokines *CXCL1*, *CXCL2*, and *CXCL8* (Supplemental Figure 8E-F), which in turn may promote NETosis, a prominent feature of HS inflammation (36, 44). In addition, this population demonstrated the most prominent expression of multiple MMPs, likely contributing to tissue destruction through proteolysis of epithelial cell junction proteins and regulation of cell-matrix interactions. Moreover, MMPs may play a role in the immune response in HS through regulating cytokine and chemokine activity and gradient formation (45). This broad inflammatory contribution of *CXCL13*$^+$ fibroblast to HS pathogenesis identifies this subtype as a potential target to alter the chronic inflammatory response in HS.

In addition to prominent immune cell infiltration, fibrosis is a hallmark of longstanding HS. Our study implicates another HS-associated FB subtype in this process; the *SFRP4*$^{+}$ myofibroblasts, whose primary function, the production of extracellular matrix (ECM) components, was found to be driven by Hippo pathway signaling, a pro-fibrotic pathway in HS pathogenesis. The Hippo pathway is a highly conserved pathway that has been shown to play a central role in regulating cell proliferation and tissue regeneration (46). Increased activation of this pathway has been shown to play a pivotal role in fibrotic diseases such as idiopathic pulmonary fibrosis (21), and our data further implicate this pathway in HS fibrosis (Figure 7). Central to Hippo signaling is a kinase cascade, wherein MST1/2 and SAV1 form a complex to phosphorylate and activate LATS1/2 (Figure 7A) (47). LATS1/2 kinases in turn phosphorylate the transcriptional co-activators YAP and TAZ, resulting in sequestration of the YAP/TAZ complex in the cytoplasm and subsequent degradation. When dephosphorylated, however, the YAP/TAZ complex translocates into the nucleus where it interacts with the transcriptional factors, TEAD1-4, to promote the expression of multiple genes associated with cell proliferation, myofibroblast development, and collagen deposition (47). In HS FBs, treatment with verteporfin, which inhibits transcriptional activity of the Hippo pathway through disruption of the interaction between YAP/TAZ and TEAD1-4, reduced both the myofibroblast phenotype and collagen production, whereas the opposite response was seen with TRULI, which promotes translocation of YAP into the nucleus promoting binding with TEAD transcriptional factors (Figure 7B-F). Notably, however, Hippo pathway modulation had minimal effect on pro-inflammatory responses of HS fibroblasts, suggesting that fibrosis can be uncoupled from the inflammatory response in HS (Figure 7G).

Currently, compounds are in development targeting the Hippo pathway for both the treatment of cancer (though inhibition of YAP/TAZ) and for wound healing and tissue regeneration (through activation of YAP/TAZ) (22). A recent mouse study showed how activation of Gα-coupled dopamine receptor D1 inhibits YAP/TAZ function in mesenchymal cells, reversing *in vitro* ECM stiffening and *in vivo* lung and liver fibrosis (48). This demonstrates that these compounds can potentially be leveraged for use in fibrotic diseases, potentially providing future treatment options for extensive and debilitating HS-associated fibrosis. Ultimately, treatment of HS is likely to be a combination of compounds with anti-inflammatory and potentially anti-fibrotic effects.

Our study does have several limitations. First, due to the scRNAseq protocol used, we were unable to efficiently capture neutrophils in our scRNA-seq analysis. Neutrophils are known to play an important role in the pathogenesis of HS, which was supported by the expression of a wide range of neutrophil-attracting and activating molecules by several different cell types. In line with this, to generate single-cell data, tissue is removed from its micro-environment and subjected to several lysis steps and mechanical stress, potentially altering the gene expression of the cells. This highlights the importance of substantiating scRNAseq findings by *in situ* methods such as spatial transcriptomics and IHC. Finally, the samples used and therefore the results found in this study are representative of only a subset of patients with HS: those with moderate-to-severe disease characterized by chronic inflammation, tissue destruction, and fibrosis. Future studies including samples from both acute and chronic lesions could help elucidate the pathways involved in disease onset and progression and identify valuable new therapeutic targets across the HS disease timeline.

Taken together, the data presented here provides an unprecedented view of the pathogenesis of chronic HS, characterizes the main cellular players, and defines their interactions. It describes a striking layering of the chronic HS infiltrate and identifies the contribution of FB subtypes in orchestrating this compartmentalized immune response. It further demonstrates the central role of the Hippo pathway in promoting the extensive fibrosis characteristic of HS and provides pre-clinical evidence that the pro-fibrotic FB response in HS can be modulated through inhibition of this pathway. These data provide insights into key aspects of HS pathogenesis with broad therapeutic implications.

METHODS

Human skin samples for single cell analyses

Five patients with chronic HS and eight healthy controls were recruited for single cell analysis at the University of Michigan, Ann Arbor, MI, USA. HS patients had a disease duration of at least 1 year prior to sampling and Hurley stage II or III disease. Patients did not use biologics or IV treatment and were off any other systemic treatment and off any topical agents for at least 2 weeks prior to inclusion. 6-mm punch biopsies were taken from lesional skin in case of HS patients and healthy control skin from the hip/buttock for healthy controls.

Single-cell RNA sequencing library preparation, sequencing, and alignment

Generation of single-cell suspensions for single-cell RNA-sequencing (scRNA-seq) was performed on 6-mm biopsies obtained from HS and healthy donors. Samples were incubated overnight in 0.4% dispase (Life Technologies) in Hank's Balanced Saline Solution (Gibco) at 4°C. Epidermis and dermis were separated. Epidermis was digested in 0.25% Trypsin-EDTA (Gibco) with 10U/mL DNase I (Thermo Scientific) for 1 hour at 37°C, quenched with FBS (Atlanta Biologicals), and strained through a 70μM mesh. Dermis was minced, digested in 0.2% Collagenase II (Life Technologies) and 0.2% Collagenase V (Sigma) in plain medium for 1.5 hours at 37°C, and subsequently strained through a 70μM mesh. Epidermal and dermal cells were combined in 1:1 ratio and libraries were constructed by the University of Michigan Advanced Genomics Core on the 10X Chromium system with chemistry v2 and v3. Libraries were then sequenced on the Illumina NovaSeq 6000 sequencer to generate 150bp paired-end reads. Data processing including quality control, read alignment (hg38), and gene quantification was conducted using the 10X Cell Ranger software. The samples were then merged into a single

expression matrix using the cellranger aggr pipeline. See Supplemental methods for information on cell clustering, cell-type annotation, ligand-receptor analysis, pseudotime-trajectory construction, and spatial transcriptomic analyses.

Isolation of primary dermal fibroblasts

HS fibroblasts were cultured from routinely excised chronic lesional skin at the Erasmus University Medical Center, Rotterdam, the Netherlands (Supplemental Table 1). Fibroblasts were obtained by dissecting and mincing the dermis from excised skin. Minced tissue was placed in DMEM (Lonza BioWhittaker®) containing 20% FBS (Gibco, V/V), L-Glutamine (mM), and Penicillin/Streptomycin (Lonza BioWhittaker®, 10.000U) and incubated in 5% CO2 at 37°C until fibroblast colony formation was observed. At 75-80% confluency, the fibroblasts were trypsinized with a Trypsin/EDTA solution (Cat No. CC-5012; Lonza), incubated at 37°C for 5–10 minutes. Trypsin was blocked with DMEM containing 10% FBS and centrifuged at xxx for 10 minutes at RT for subsequent subculture or cryopreservation. Cryopreserved HS FBs with passage numbers ≤3 were shipped to the University of Michigan and used for functional experiments. In addition, healthy donors were recruited from the Department of Dermatology of the University of Michigan and dermal fibroblasts were isolated from punch biopsies from the hip/buttock. Healthy controls were age and gender matched to the HS patients. Gene expression changes between healthy donor and HS fibroblasts were analyzed by quantitative PCR after total RNA was extracted using the RNA plus easy mini kit (QIAGEN) and cDNA was synthesized with the Applied Biosystems™ High-Capacity cDNA Reverse Transcription Kit. Quantitative PCR was performed in a 7900HT Fast Real-Time PCR System.

Fibroblast treatment and functional experiments

Dermal fibroblasts from HS patients were treated with 10 µM of LATS kinase inhibitor TRULI/Lats-IN-1 (MedChenExpress HY-138489) or YAP/TEAD inhibitor verteporfin (Cayman Chemical 17334) 0.1- 10 µM for 48 to 72 hours. Additional 6-hour cytokine stimulations were performed using IL-1β (10ng/ml, 201-LB-005) and TNFα (10ng/ml, 210-TA-005). Gene expression changes in cells were performed by qPCR after total RNA was extracted using Direct-zol™ RNA MiniPrep Kit (Zymo Research R2052). Quantitative PCR was performed in a ViiA™ 7 Real-Time PCR System. Protein expression changes was monitored using Western blotting. After blocking, the blots were probed with antibodies against collagen I (COL1, ab6308) or αSMA (ab5694). For loading control, the blots were immunoblotted with antibodies against GAPDH (Cell Signaling #2118). Band quantification was performed using ImageJ (49). The IncuCyte® Live-Cell Imaging System was used to monitor cell proliferation or migration. After adding different treatments cells were monitored by IncuCyte®. Cell counts were analyzed by the IncuCyte® S3 Analysis software. Gel contraction assays was performed using the cell contraction kit from Cell Biolabs (CBA-201).

Statistical analysis *in vitro* experiments

For the *in vitro* experiments, normality was assessed using the Shapiro-Wilks test. To determine the differences between groups one-way ANOVA (post hoc Dunnett's test) or Kruskal–Wallis tests (post hoc Dunn's test) were performed For time curve experiments a repeated measures two-way ANOVA (with post hoc two-stage step-up method of Benjamini, Krieger and Yekutieli (50) to control the false discovery rate) were performed. All analyses were performed using

GraphPad Prism version 8 (GraphPad Software, Inc). Tests were two-sided and p-values of less than 0.05 were considered statistically significant.

Study approval

The study was approved by the University of Michigan institutional review board (HUM00174864), and all patients provided written, informed consent.

Data availability

The scRNAseq data discussed in this publication have been deposited in NCBI's Gene Expression Omnibus (GEO) and are accessible through GEO Series accession numbers GSE154775 and GSE173706 (https://www.ncbi.nlm.nih.gov/geo/query/acc.cgi?acc=GSE154775; https://www.ncbi.nlm.nih.gov/geo/query/acc.cgi?acc=GSE173706). Data from other experiments and analyses used to generate the figures can be found in the “Supporting data values” XLS file.

ACKNOWLEDGMENTS

This work was supported by a Rubicon Fellowship of The Netherlands Organisation for Health Research and Development (ZonMw, KRvS). This work was supported by a research grant from Almirall with additional support by the Babcock Endowment Fund (LCT, JEG), by the National Institute of Health: R01-AR069071 and R01-AR073196 (JEG), P30-AR075043 (JEG, LCT), K01-AR072129 (LCT), R01-AI022553, R01-AR040312, R01-AR074302 and R01-AR074302 (RLM), and the A. Alfred Taubman Medical Research Institute (JEG, JMK). ACB is supported by the Dermatology Foundation. LCT is supported by the Dermatology Foundation, Arthritis

National Research Foundation, and National Psoriasis Foundation. MKS is supported by National Psoriasis Foundation. We would like to thank prof. Errol P. Prens for continuing to provide support and guidance to the first author. In addition, we would like to acknowledge both prof. Errol P. Prens and dr. Hessel H. van der Zee for providing HS tissue samples used for HS fibroblast isolations.

AUTHOR CONTRIBUTIONS

Conceptualization: KRvS, JEG. *Investigation:* KRvS, PST, OP, MGK, WW, MKS, RU, MN, ME, CW, CB, HK, JCB, WDB, MNM. *Formal analysis:* KRvS, FM, PST, RW, LCT. *Visualization:* KRvS, FM, RW, LCT. *Funding acquisition:* KRvS, LCT, JEG, JMK. *Supervision:* JEG. *Writing – original draft*: KRvS, JEG. *Writing – review & editing:* KRvS, FM, PST, OP, MGK, MC, XX, MKS, RU, PWH, RW, LN, MN, ME, CW, CD, JHK, JCB, WDB, KW, ÖU, MNM, MP, RLM, EM, RS, JMK, ACB, LCT, JEG.

REFERNCES

1. Jfri A, et al. Prevalence of hidradenitis suppurativa: A systematic review and meta-regression analysis. *JAMA Dermatol*. 2021;157(8):924–931.

2. van Straalen KR, Prens EP, Gudjonsson JE. Insights into hidradenitis suppurativa. *J Allergy Clin Immunol*. 2022;149(4):1150–1161.

3. Sabat R, et al. Hidradenitis suppurativa. *Nat Rev Dis Primers*. 2020;6(1):18.

4. van Straalen KR, et al. Contribution of genetics to the susceptibility to hidradenitis suppurativa in a large, cross-sectional Dutch twin cohort. *JAMA Dermatol*. 2020;156(12):1359–1362.

5. Jemec GB, Heidenheim M, Nielsen NH. The prevalence of hidradenitis suppurativa and its potential precursor lesions. *J Am Acad Dermatol*. 1996;35(2 Pt 1):191–194.

6. Kjaersgaard Andersen R, et al. Evidence of gene-gene interaction in hidradenitis suppurativa: a nationwide registry study of Danish twins. *Br J Dermatol*. 2022;186(1):78–85.

7. Castelli E, et al. Histopathological progression of hidradenitis suppurativa/acne inversa : A morphological study with a closer look on the early changes of the folliculosebaceous apocrine apparatus. *Wien Med Wochenschr*. 2022;172(5–6):126–134.

8. van der Zee HH, et al. Alterations in leucocyte subsets and histomorphology in normal-appearing perilesional skin and early and chronic hidradenitis suppurativa lesions. *Br J Dermatol*. 2012;166(1):98–106.

9. Gudjonsson JE, et al. Contribution of plasma cells and B cells to hidradenitis suppurativa pathogenesis. *JCI Insight*. 2020;5(19):139930.

10. Kimball AB, et al. Two phase 3 trials of adalimumab for hidradenitis suppurativa. *N Engl J Med*. 2016;375(5):422–434.

11. Glatt S, et al. Efficacy and safety of bimekizumab in moderate to severe hidradenitis suppurativa: A phase 2, double-blind, placebo-controlled randomized clinical trial. *JAMA Dermatol*. 2021;157(11):1279–1288.

12. Witte-Händel E, et al. The IL-1 pathway is hyperactive in hidradenitis suppurativa and contributes to skin infiltration and destruction. *J Invest Dermatol*. 2019;139(6):1294–1305.

13. Wolk K, et al. Activity and components of the granulocyte colony-stimulating factor pathway in hidradenitis suppurativa. *Br J Dermatol*. 2021;185(1):164–176.

14. Mantovani A, Bonecchi R, Locati M. Tuning inflammation and immunity by chemokine sequestration: decoys and more. *Nat Rev Immunol*. 2006;6(12):907–918.

15. Bonecchi R, Graham GJ. Atypical chemokine receptors and their roles in the resolution of the inflammatory response. *Front Immunol*. 2016;7:224.

16. Lowe MM, et al. Immunopathogenesis of hidradenitis suppurativa and response to anti-TNF-α therapy. *JCI Insight*. 2020;5(19):139932.

17. Moran B, et al. Hidradenitis suppurativa is characterized by dysregulation of the Th17:Treg cell axis, which is corrected by anti-TNF therapy. *J Invest Dermatol*. 2017;137(11):2389–2395.

18. Yoshitomi H, Ueno H. Shared and distinct roles of T peripheral helper and T follicular helper cells in human diseases. *Cell Mol Immunol*. 2021;18(3):523–527.

19. Lion J, et al. HLA Class II antibody activation of endothelial cells promotes Th17 and disrupts regulatory T lymphocyte expansion. *Am J Transplant*. 2016;16(5):1408–1420.

20. Tabib T, et al. SFRP2/DPP4 and FMO1/LSP1 define major fibroblast populations in human skin. *J Invest Dermatol*. 2018;138(4):802–810.

21. Tang W, et al. Hippo signaling pathway and respiratory diseases. *Cell Death Discov*. 2022;8(1):213.

22. Dey A, Varelas X, Guan K-L. Targeting the Hippo pathway in cancer, fibrosis, wound healing and regenerative medicine. *Nat Rev Drug Discov*. 2020;19(7):480–494.

23. Wang J, et al. The Hippo pathway in the heart: pivotal roles in development, disease, and regeneration. *Nat Rev Cardiol*. 2018;15(11):672–684.

24. Dostal D, Glaser S, Baudino TA. Cardiac fibroblast physiology and pathology. *Compr Physiol*. 2015;5(2):887–909.

25. Kastan N, et al. Small-molecule inhibition of Lats kinases may promote Yap-dependent proliferation in postmitotic mammalian tissues. *Nat Commun*. 2021;12(1):3100.

26. Shi-Wen X, et al. Verteporfin inhibits the persistent fibrotic phenotype of lesional scleroderma dermal fibroblasts. *J Cell Commun Signal*. 2021;15(1):71–80.

27. Strieter RM, Gomperts BN, Keane MP. The role of CXC chemokines in pulmonary fibrosis. *J Clin Invest*. 2007;117(3):549–556.

28. Mehrad B, Keane MP, Strieter RM. Chemokines as mediators of angiogenesis. *Thromb Haemost*. 2007;97(5):755–762.

29. Carvalheiro T, et al. Induction of inflammation and fibrosis by semaphorin 4A in systemic sclerosis. *Arthritis Rheumatol*. 2019;71(10):1711–1722.

30. Juhl P, et al. Dermal fibroblasts have different extracellular matrix profiles induced by TGF-β, PDGF and IL-6 in a model for skin fibrosis. *Sci Rep*. 2020;10(1):17300.

31. Devocelle A, et al. IL-15 prevents renal fibrosis by inhibiting collagen synthesis: A new pathway in chronic kidney disease? *Int J Mol Sci*. 2021;22(21):11698.

32. de la Rosa G, et al. Migration of human blood dendritic cells across endothelial cell monolayers: adhesion molecules and chemokines involved in subset-specific transmigration. *J Leukoc Biol*. 2003;73(5):639–649.

33. Fahey E, Doyle SL. IL-1 family cytokine regulation of vascular permeability and angiogenesis. *Front Immunol*. 2019;10:1426.

34. Dees C, et al. Notch signalling regulates fibroblast activation and collagen release in systemic sclerosis. *Ann Rheum Dis*. 2011;70(7):1304–1310.

35. Burn GL, et al. The Neutrophil. *Immunity*. 2021;54(7):1377–1391.

36. Byrd AS, et al. Neutrophil extracellular traps, B cells, and type I interferons contribute to immune dysregulation in hidradenitis suppurativa. *Sci Transl Med*. 2019;11(508):eaav5908.

37. Leal Rojas IM, et al. Human blood CD1c+ dendritic cells promote Th1 and Th17 effector function in memory CD4+ T cells. *Front Immunol*. 2017;8:971.

690 38. Della-Torre E, et al. B lymphocytes directly contribute to tissue fibrosis in patients with
691 IgG4-related disease. *J Allergy Clin Immunol*. 2020;145(3):968-981.e14.

692 39. Barone F, et al. Stromal fibroblasts in tertiary lymphoid structures: A novel target in chronic
693 inflammation. *Front Immunol*. 2016;7:477.

694 40. Cosgrove J, et al. B cell zone reticular cell microenvironments shape CXCL13 gradient
695 formation. *Nat Commun*. 2020;11(1):3677.

696 41. Luo S, et al. Chronic inflammation: A common promoter in tertiary lymphoid organ
697 neogenesis. *Front Immunol*. 2019;10:2938.

698 42. Nayar S, et al. Immunofibroblasts are pivotal drivers of tertiary lymphoid structure formation
699 and local pathology. *Proc Natl Acad Sci U S A*. 2019;116(27):13490–13497.

700 43. Dieu-Nosjean M-C, et al. Tertiary lymphoid structures in cancer and beyond. *Trends*
701 *Immunol*. 2014;35(11):571–580.

702 44. Kaplan MJ, Radic M. Neutrophil extracellular traps: double-edged swords of innate
703 immunity. *J Immunol*. 2012;189(6):2689–2695.

704 45. Manicone AM, McGuire JK. Matrix metalloproteinases as modulators of inflammation.
705 *Semin Cell Dev Biol*. 2008;19(1):34–41.

706 46. Zhao B, Tumaneng K, Guan K-L. The Hippo pathway in organ size control, tissue
707 regeneration and stem cell self-renewal. *Nat Cell Biol*. 2011;13(8):877–883.

708 47. Mia MM, Singh MK. New insights into Hippo/YAP signaling in fibrotic diseases. *Cells*.
709 2022;11(13):2065.

48. Haak AJ, et al. Selective YAP/TAZ inhibition in fibroblasts via dopamine receptor D1 agonism reverses fibrosis. *Sci Transl Med*. 2019;11(516):eaau6296.

49. Schneider CA, Rasband WS, Eliceiri KW. NIH Image to ImageJ: 25 years of Image Analysis. *Nat Methods*. 2012;9(7):671–675.

50. Benjamini Y, Krieger AM, Yekutieli D. Adaptive linear step-up procedures that control the false discovery rate. *Biometrika*. 2006;93(3):491–507.

FIGURES

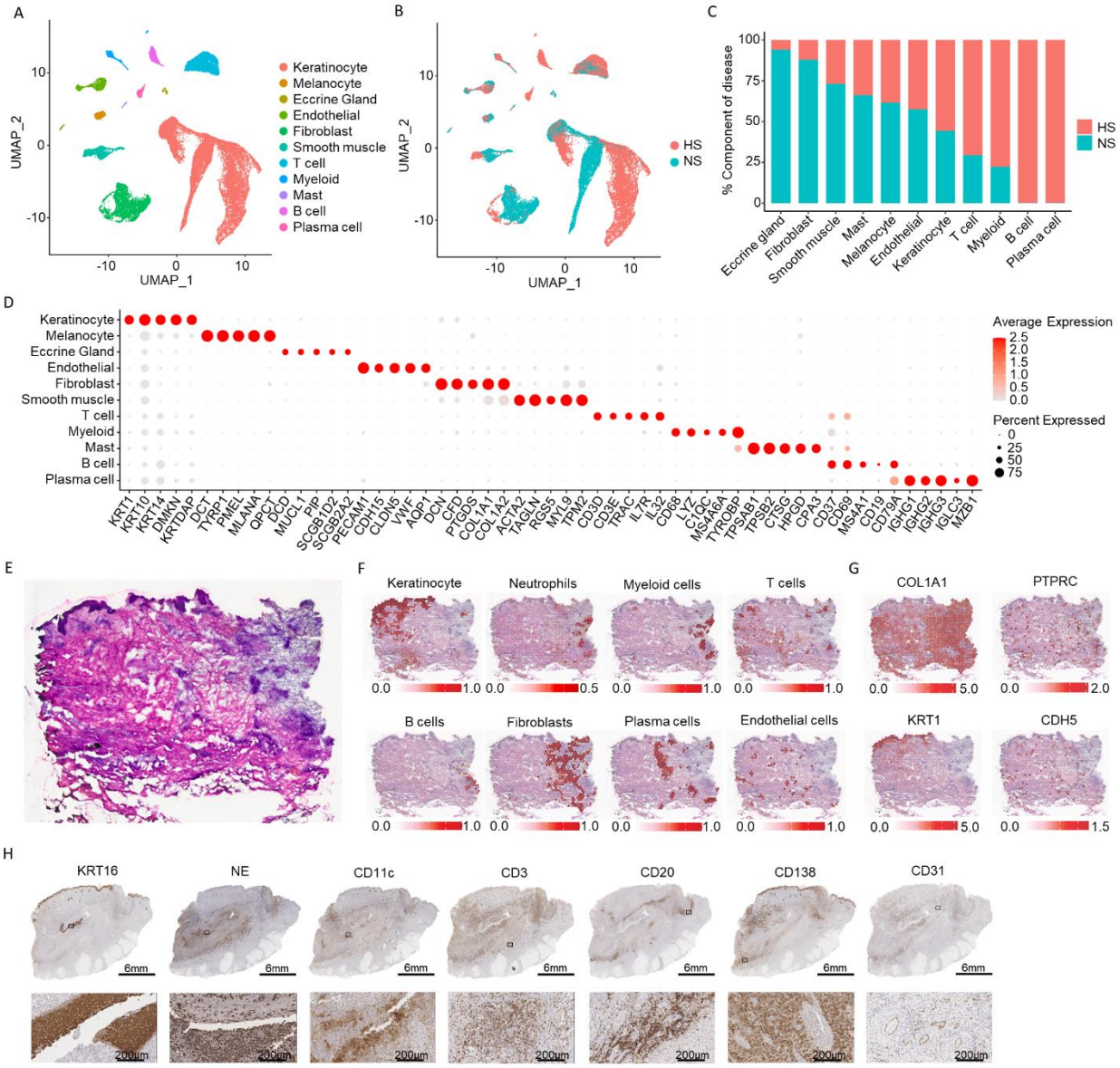

Figure 1. Cell types observed in hidradenitis suppurativa lesional skin and their spatial locations. **(A)** UMAP plot showing 31,746 cells colored by cell types. **(B)** UMAP plot showing the cells colored by disease conditions. HS: hidradenitis suppurativa; NS: normal skin from healthy controls. **(C)** Bar chart showing the cell types as percentage component of disease. **(D)** Dot plot showing five representative marker genes for each cell type. The color scale represents the scaled expression average of each gene. The size of the dot represents the percentage of cells expressing each gene. **(E)** H & E staining of the biopsy used for spatial transcriptomics. **(F)** Spatial plot showing localization of keratinocytes, neutrophils, myeloid cells, fibroblasts, B cells, plasma cells, and endothelial cells superimposed on H&E slide. **(G)**

Spatial plot showing detection of *COL1A1* (encoding Collagen 1A1), *PTPRC* (CD45), *KRT1* (Keratin 1) and *CDH5* (Cadherin 5) within HS lesional skin. **(H)** Immunohistochemistry showing the localization of proliferative keratinocytes (KRT16), neutrophils (NE; neutrophil elastase) T-cells (CD3), B cells (CD20), plasma cells (CD138), dendritic cells (CD11c), and endothelial cells (CD31) in HS lesional skin (patient HS1).

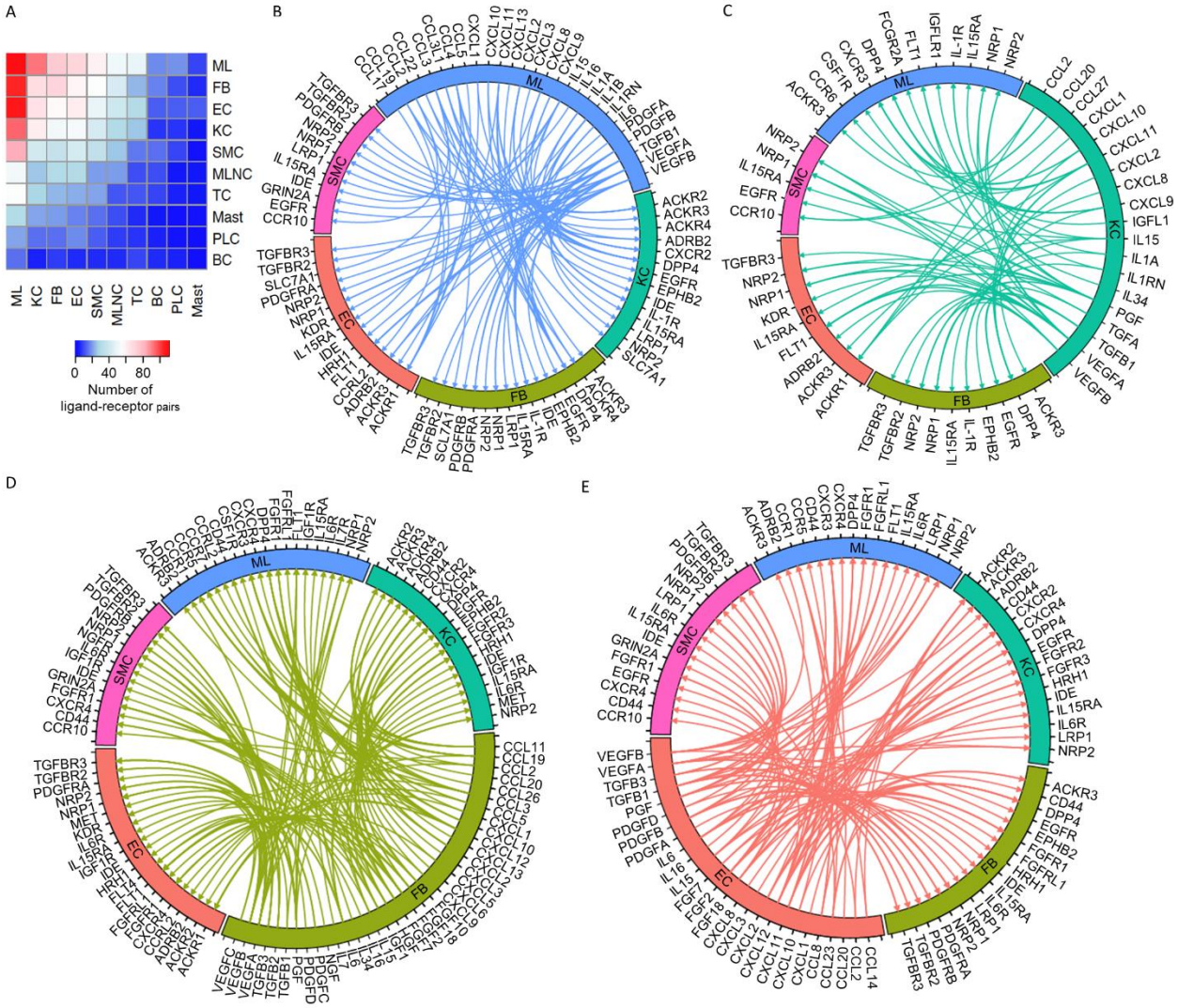

Figure 2. Ligand-receptor interactions between cell types.
(A) Heatmap showing the number of ligand-receptor pairs with a higher score in HS compared to NS among the cell types. Row, cell type expressing ligand; column, cell type expressing receptor. ML, myeloid cells; FB, fibroblasts; EC, endothelial cells; KC, keratinocytes; SMC, smooth muscle cells; MLNC, melanocytes; TC, T cells; Mast, mast cells; PLC, plasma cells; BC, B cells. **(B-E)** Circos plots showing cytokine and

growth factor ligand-receptor interactions with higher scores in HS compared with NS in which ligands are expressed by **(B)** myeloid cells, **(C)** keratinocytes, **(D)** fibroblasts, and **(E)** endothelial cellswith receptors expressed by other cell types.

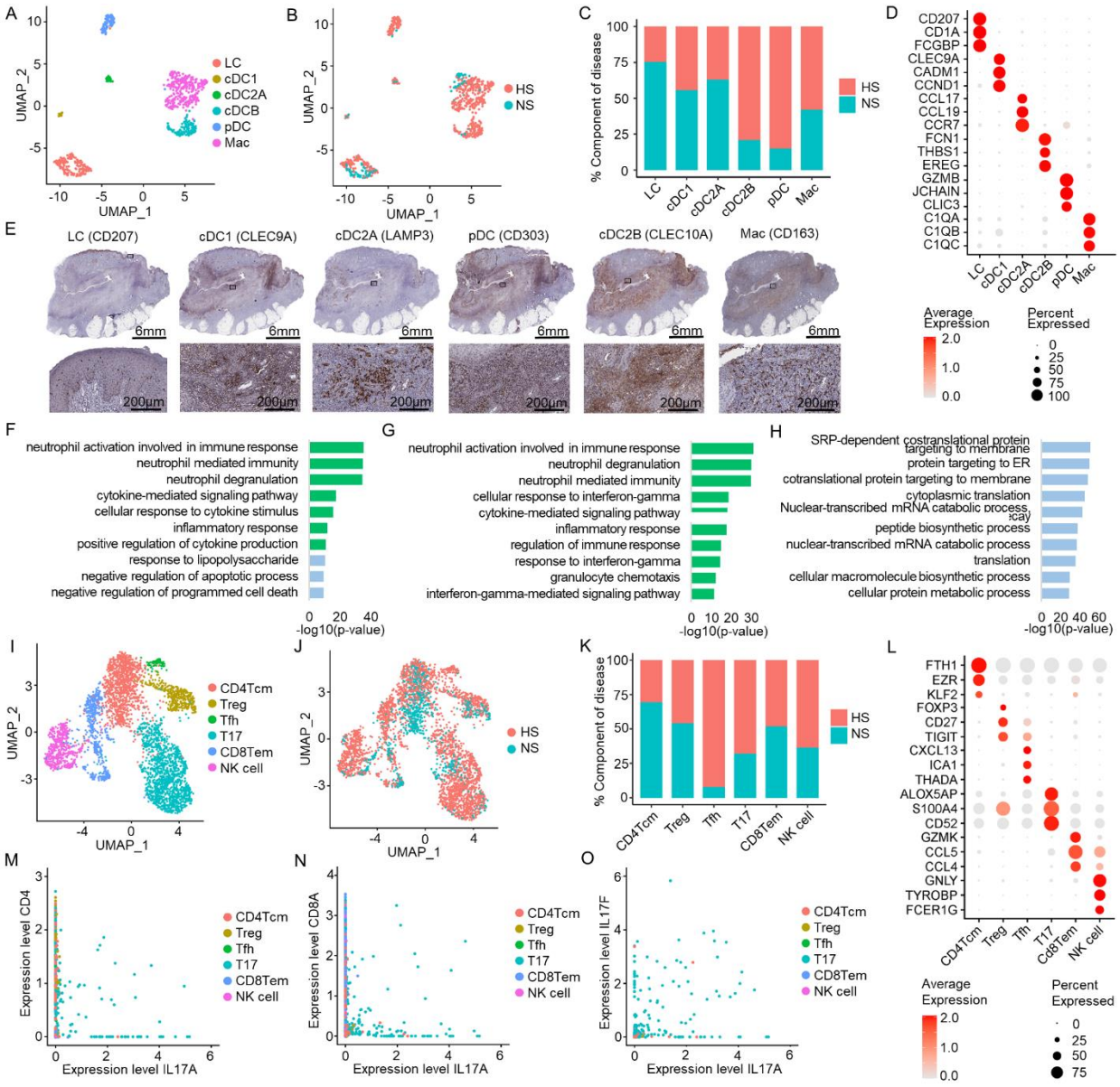

Figure 3. Identification of myeloid cells and T cells subsets in HS lesional skin.
(A) UMAP showing 689 myeloid cells colored by subtypes. **(B)** UMAP showing the cells colored by disease conditions. **(C)** Bar chart showing the subtypes as percentage component of disease. **(D)** Dot plot showing representative marker genes for each subtype. Color represents scaled expression; size of the dot represents the percentage of cells expressing the gene. **(E)** Immunohistochemistry showing myeloid cell subtype localization in HS lesional skin (patient HS1). **(F)** Bar chart showing enriched Gene Ontology Biological Processes in HS cDC2B cells, macrophages **(G)**, and pDC **(H)**; green, immune associated; blue, transcription related and other BPs. **(I)** UMAP showing 3985 T cells colored by subtypes. **(J)** UMAP showing T cells colored by disease conditions. **(K)** Bar chart showing the T cell subtypes as percentage component of disease. **(L)** Dot plot showing representative marker genes for T cell subtypes. Color represents scaled expression; size of the dot represents the percentage of cells expressing the gene. **(M, N)** Scatter plot showing the correlation between the level of expression of IL-17A (x-axis) and CD4 **(M,** ρ=0.03**)** or CD8A **(N,** ρ=0.01**)**. **(O)** Scatter plot showing the correlation between the level of expression of IL-17A and IL-17F, ρ=0.44, among T cells.

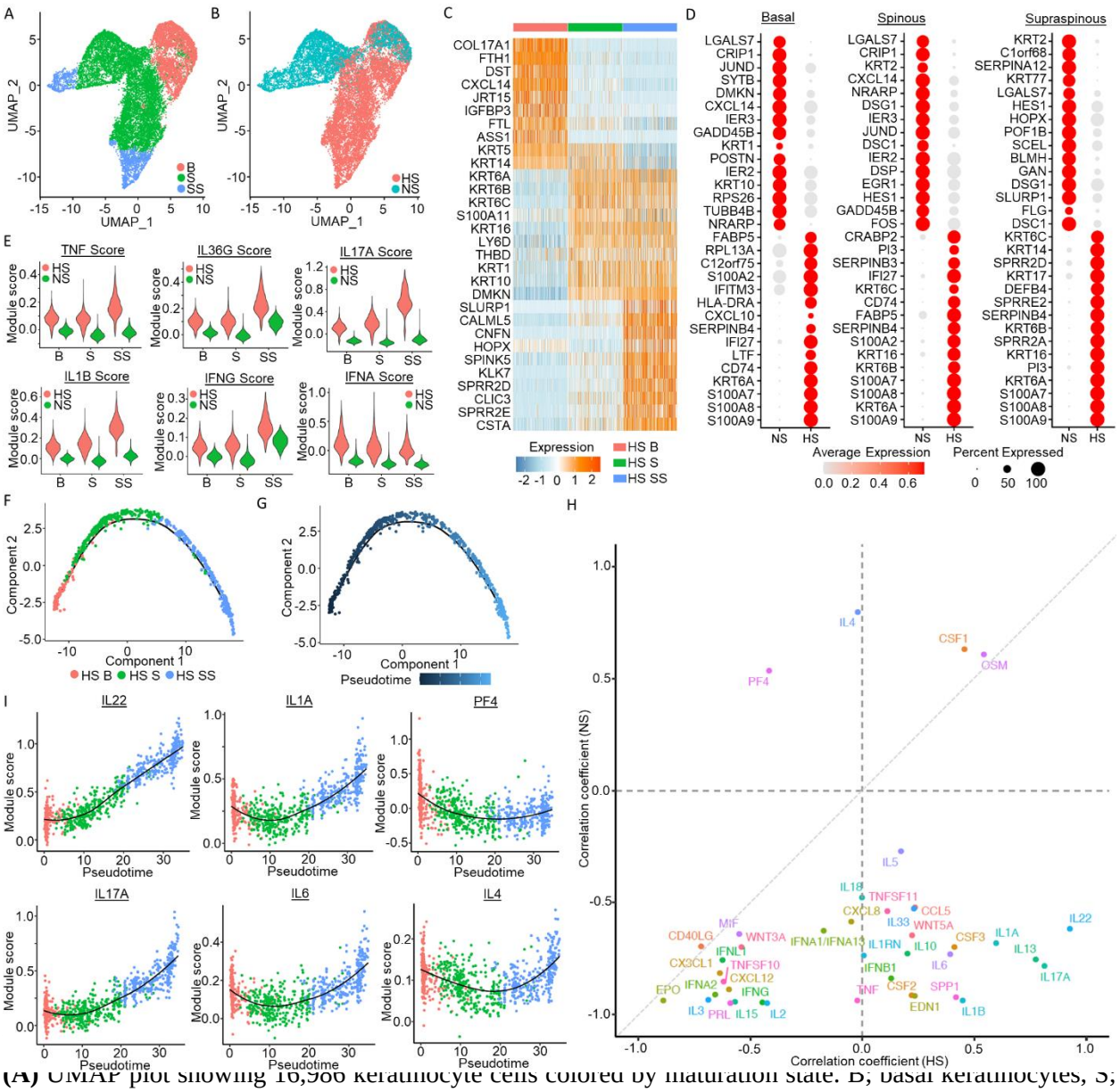

(A) UMAP plot showing 16,986 keratinocyte cells colored by maturation state. B; basal keratinocytes, S; spinous keratinocytes, SS; supraspinous keratinocytes **(B)** UMAP plot showing the keratinocytes colored by disease conditions. **(C)** Heatmap showing marker genes with the highest fold change for each subtype. HS; hidradenitis suppurativa, NS; healthy control. **(D)** Dot plot showing the top 15 differentially expressed genes comparing HS to NS in the basal (left), spinous (middle) and supraspinous (right) layer. The color scale represents the scaled expression, and the size of the dot represents the percentage of keratinocytes expressing of each gene. **(E)** Violin plot showing the cytokine module scores in the keratinocyte subtypes, split for HS (red) and NS (green). **(F)** Pseudotime trajectory colored by the subtype identity of HS keratinocytes. **(G)** Pseudotime trajectory colored by the pseudotime of the HS keratinocytes. Dark blue represents early, light blue represents late. **(H)** Scatter plot showing the correlation between upstream regulators for HS and NS keratinocytes. **(I)** Scatter plot showing the correlation between HS-derived keratinocyte pseudotimes and module scores for IL17A, IL22, IL1A, IL6 calculated using genes induced in cultured keratinocytes stimulated by individual cytokines. The color represents the pseudotime subtype identity of the cell.

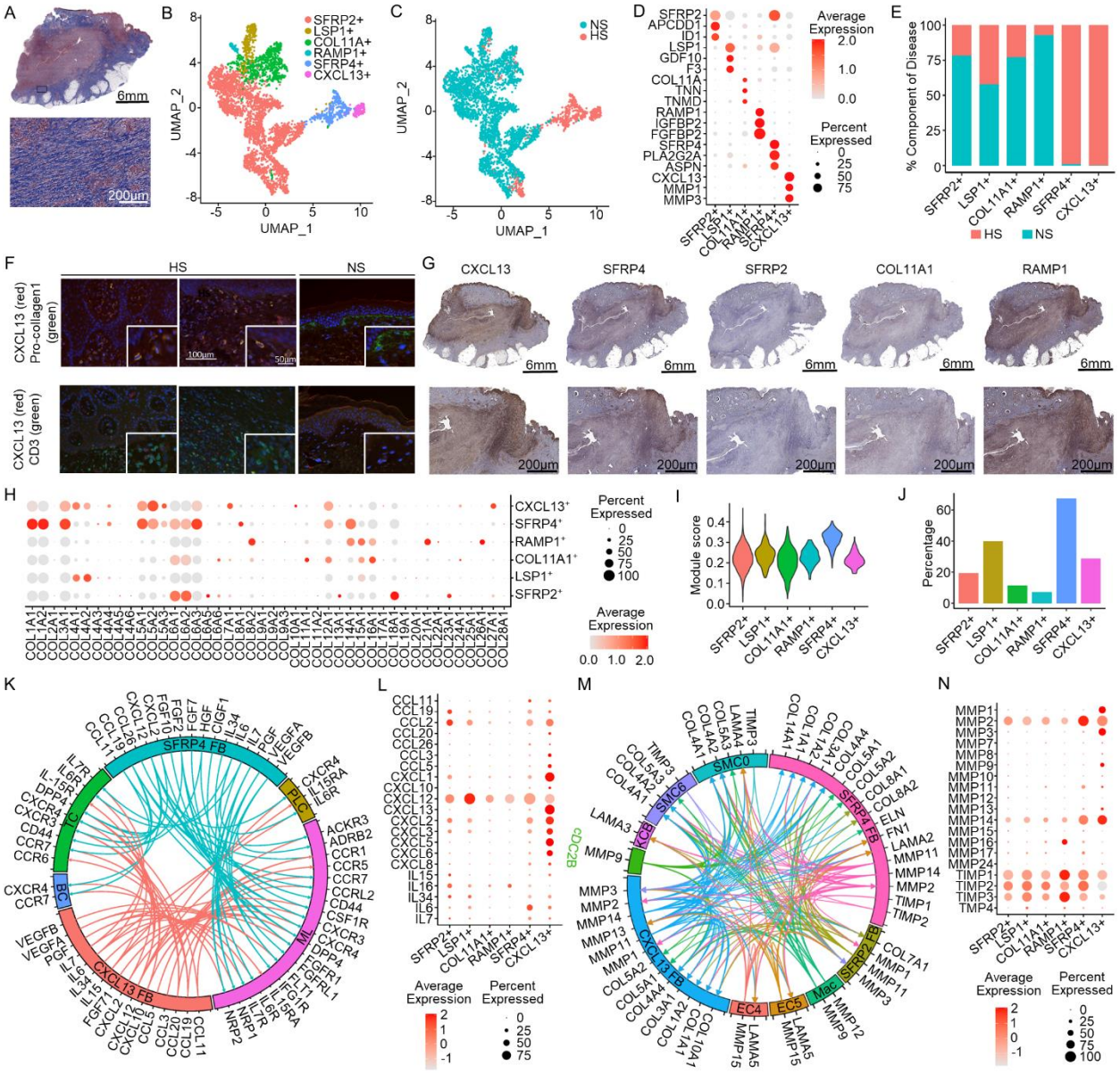

Figure 5. Identification of HS-associated fibroblast subsets.

(A) Trichrome staining of HS lesional skin (patient HS1); blue, collagen. **(B)** UMAP plot showing 4,459 fibroblasts colored by subtypes: Secreted Frizzled Related Protein 2 (SFRP2^{+}), Lymphocyte Specific Protein 1 (LSP1^{+}). Collagen Type XI Alpha 1 Chain (COL11A1^{+}), Receptor Activity Modifying Protein 1 (RAMP1^{+}), Secreted Frizzled Related Protein 4 (SFRP4^{+}), C-X-C Motif Chemokine Ligand 13 (CXCL13^{+}). **(C)** UMAP plot showing the cells colored by disease conditions. HS; hidradenitis suppurativa, NS; healthy control. **(D)** Dot plot showing the representative marker genes for each subtype. Color scale represents scaled expression, size of the dot represents the percentage of cells expressing the gene. **(E)** Bar chart showing the cell types as percentage component of disease. **(F)** Immunofluorescence showing the colocalization of CXCL13 with vimentin (fibroblasts) and to a lesser extent CD3 (T cells). **(G)** Immunohistochemistry showing FB subsets in HS lesional skin (patient HS1). **(H)** Dot plot showing the expression of collagen genes for each fibroblast subtype. Color scale represents scaled expression, size of the dot represents the percentage of cells expressing the gene. **(I)** ECM module score plotted using extracellular matrix pathway gene list from Gene Ontology, ECM; extracellular matrix. **(J)** Expression of

ACTA2 among fibroblast subtypes. **(K)** Circos plot showing the cytokine and chemokine interactions from the SFRP4+ and CXCL13+ fibroblasts with other cell types: PLC; plasma cells, ML; myeloid cells, BC; B cells, TC; T cells. **(L)** Dot plot showing the expression of cytokines and chemokines among the fibroblast subsets. **(M)** Circos plot representing the interactions of MMPs, collagens and laminins between the most prominent HS-associated cell subtypes: Mac; macrophage, EC4; endothelial cell subcluster 4, EC5; endothelial cell subcluster 5, cDC2B; conventional type 2 B dendritic cells, SMC6; smooth muscle cell subcluster 6. **(N)** Dot plot showing the expression of MMPs among the fibroblast subsets.

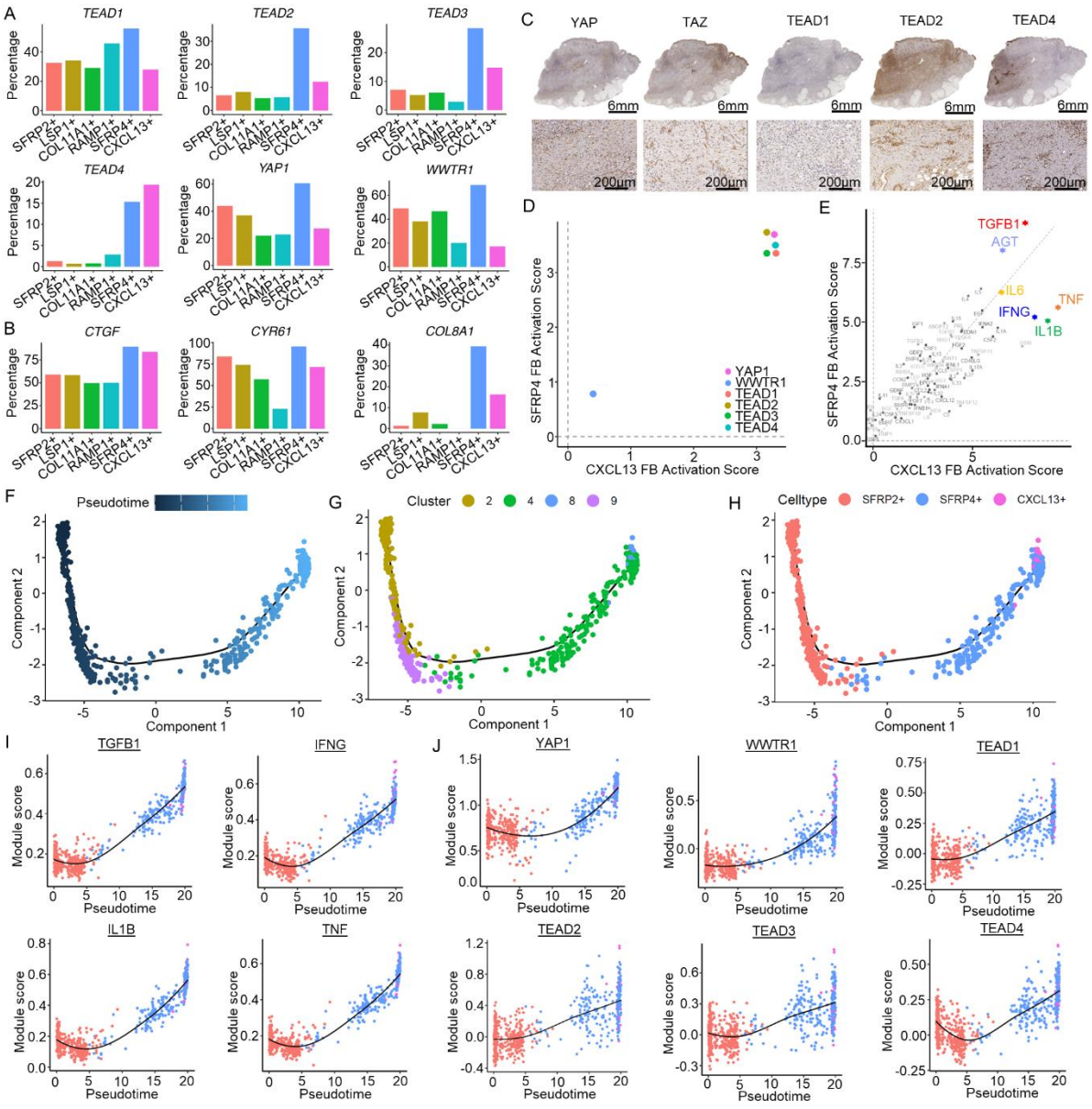

Figure 6. Expression of Hippo pathway genes their association with HS fibroblast pseudotime. **(A)** Percentage of FB subtypes expression Hippo pathway marker and target genes **(B)**. **(C)** IHC showing localization of Hippo pathway marker genes (patient HS1). **(D)** Scatter plot showing the activation z scores of Hippo pathway marker genes and activated cytokine and growth factor upstream regulators **(E)** as upstream regulators for the *SFRP4*$^{+}$ and *CXCL13*$^{+}$ FBs**. (F)** Pseudotime trajectory of HS *SFRP2*$^{+}$, *SFRP4*$^{+}$ and *CXCL13*$^{+}$ FBs colored by the pseudotime; dark blue representing early, light blue representing late pseudotime. **(G)** Pseudotime trajectory colored by the pseudotime subcluster of the FBs. **(H)** Pseudotime trajectory colored by the subtype identity of HS FBs **(I)** Scatter plot showing the correlation between the FB pseudotimes and module scores for previously identified upstream regulators and Hippo pathway associated genes **(J)**. The color represents the pseudotime subcluster identity of the cell.

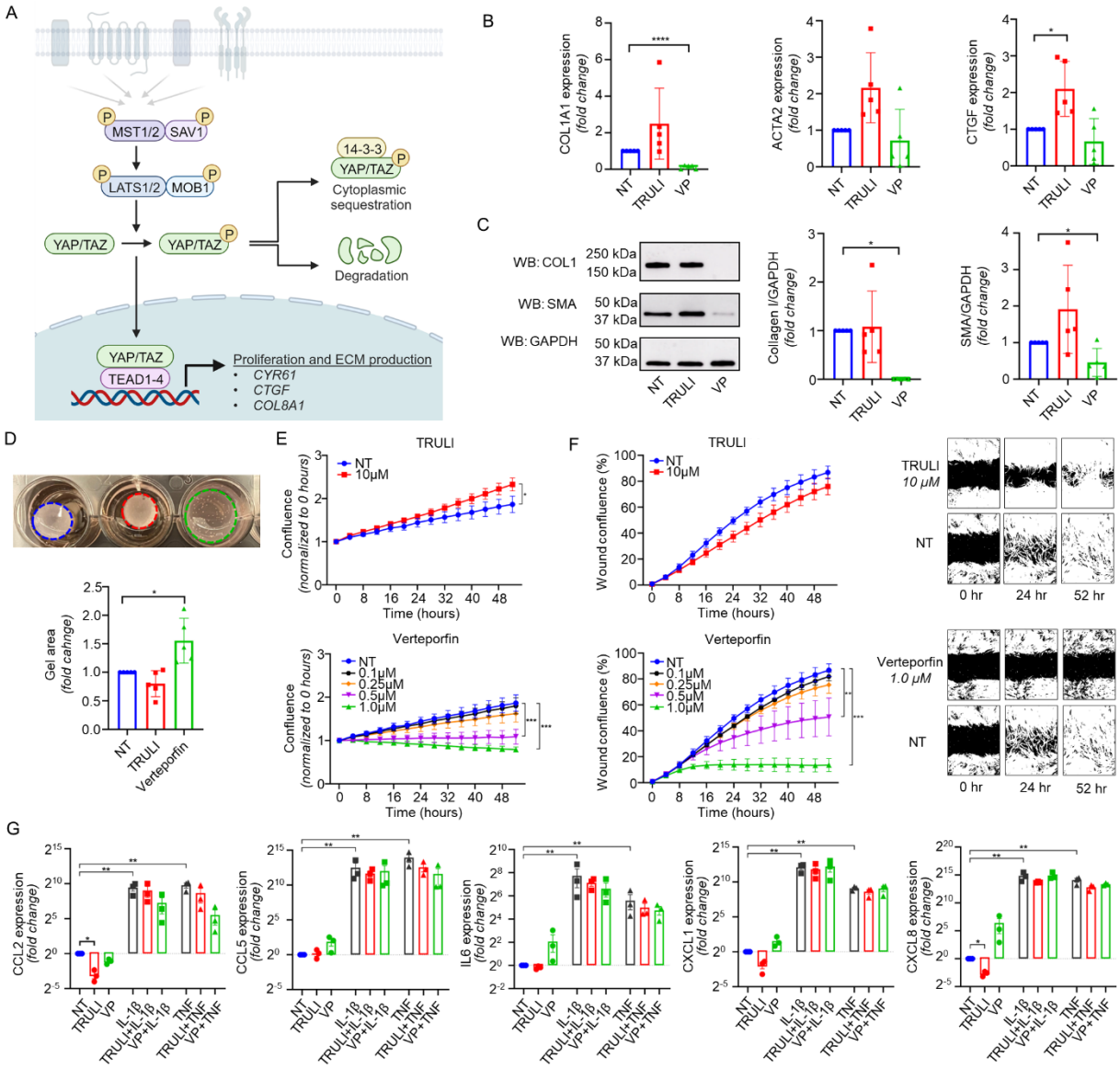

Figure 7. Modulation of the Hippo pathway in primary HS fibroblasts.

(A) Illustration of Hippo pathway, created with Biorender.com. **(B)** Quantitative PCR results showing the effect of TRULI or verteporfin (both 10 μM) on ACTA2, COL1A1, and CTGF expression in HS fibroblasts (n=5; * $p<0.05$, **** $p<0.0001$; mean ± SD; ANOVA/Kruskal-Wallis Test). **(C)** Effect of TRULI or verteporfin (both 10 μM) on smooth muscle actin (SMA) and collagen I levels in HS fibroblasts by Western blotting. n=5; *$p<0.05$; mean ± SD; Kruskal-Wallis Test (collagen I) / ANOVA (SMA). **(D)** Verteporfin blocked gel contraction in HS fibroblasts. Data normalized to the corresponding NT (untreated) group. n=5 * $p<0.05$; mean ± SD. **(E)** TRULI significantly increased cell proliferation while verteporfin dose-dependently blocked cell growth among HS fibroblasts (n=3; *$p<0.05$,***$p<0.0001$; mean ± SEM; two way repeated measures ANOVA). Same NT group shown in both panels. Cell proliferation was monitored by analyzing the occupied area by cells over time, using the IncuCyte® S3 Analysis software. **(F)** Verteporfin showed a dose-dependent reduction in cell migration of HS fibroblasts (n=3; **$p<0.01$,***$p<0.001$; mean ± SEM; two way repeated measures ANOVA). Same NT group shown in both panels. **(G)** Expression of cytokines and chemokines, among untreated (NT), IL-1β (10ng/ml) and TNFα

(10ng/ml) stimulated primary HS fibroblasts treated with or without TRULI or verteporfin treated (n=5; $p<0.05$,**$p<0.01$,***$p<0.001$; mean ± SD; one way repeated measures ANOVA).

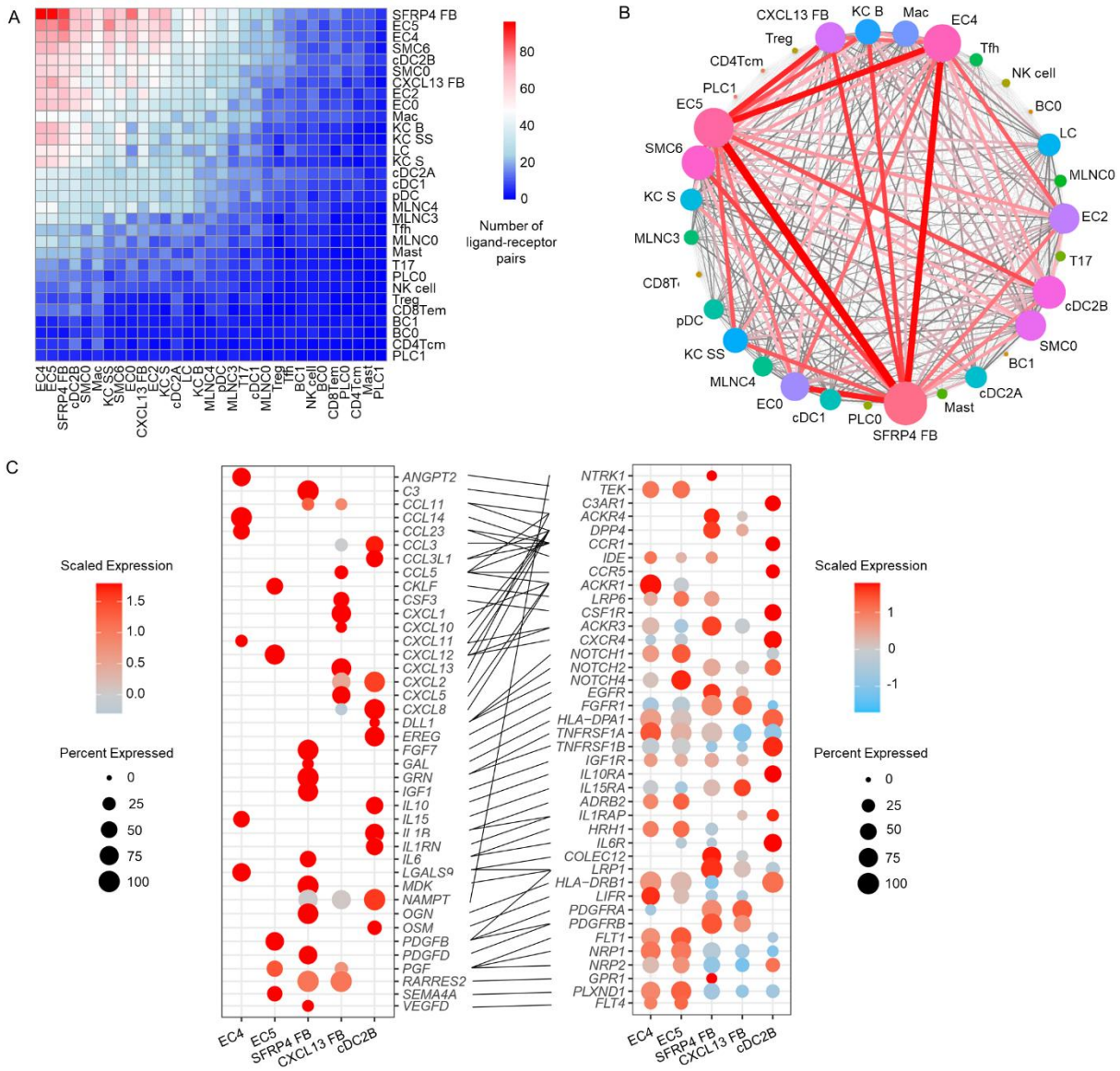

Figure 8. Ligand-receptor analysis reveals cell subtype specific networks in HS lesional skin.
(A) Heatmap showing the number of ligand-receptor pairs with a higher score in HS compared to NS among the previously identified cell subtypes. The ligands were expressed by the cell types in the row, and the receptors were expressed by the cell types in the column. The color scale represents the number of ligand receptor pairs. **(B)** Connectome web showing ligand-receptor interactions between all identified cell subsets. Thickness of the line indicates the number of interactions. **(C)** Dot plot showing selected ligand-interactions between the five most contributing cell subtypes. The color scale represents the scaled expression of the gene. The size of the dot represents the percentage of cells expressing the gene of interest, lines link the ligands to receptors.